SOCIETY FOR INFORMATION DISPLAY

2008 VEHICLES AND PHOTONS SYMPOSIUM

DIGEST OF TECHNICAL PAPERS

OCTOBER 16–17, 2008
UNIVERSITY OF MICHIGAN-DEARBORN
FAIRLANE CENTER
DEARBORN, MICHIGAN, U.S.A.

SYMPOSIUM CONFERENCE SPONSORS

DENSO

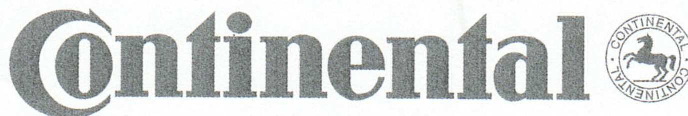

Futaba®

5.3: RF Sputter a-InGaZnO Thin Film Transistors for Flat Panel Displays

Charlene Chen[1], Katsumi Abe[2], Hideya Kumomi[2], and Jerzy Kanicki[1]*
[1]Organic and Molecular Electronics Laboratory, Department of Electrical Engineering and Computer Science
The University of Michigan, Ann Arbor, Michigan 48109, USA
[2]Canon Research Center, Canon Inc., 30-2, Shimomaruko 3-chome, Ohta-ku, Tokyo 146-8501, Japan
*Email address: Kanicki@eecs.umich.edu

Abstract: *In this paper, we studied the electrical properties of RF sputter amorphous In-Ga-Zn-O (a-InGaZnO) thin film transistors (TFTs). Several characterization methods were suggested including the extraction of the field-effect mobility, threshold voltage, nonlinear factor, and source/drain contact resistance.*

Keywords: RF sputter; amorphous In-Ga-Zn-O (a-InGaZnO); thin film transistor (TFT).

Introduction: Most flat panel displays (FPDs) currently produced are based on either low temperature polysilicon (LTPS) thin film transistors (TFTs) [1] [2] or hydrogenated amorphous silicon (a-Si:H) TFTs [3]. LTPS TFTs have high field-effect mobilities (~100cm^2/V-s) and provide both n- and p-type devices, which allow the integration of the driver circuit on the same glass substrate with the active matrix display. However, due to the relatively high fabrication cost and poor uniformity, the application of LTPS TFTs are mostly restricted to smaller format high resolution displays. On the other hand, a-Si:H technology is quite mature, and presently dominates the market of large area active-matrix liquid-crystal displays (AMLCDs). However, a-Si:H TFTs have low mobilities (~1cm^2/V-s) and suffers threshold voltage shift after prolong biases, therefore require larger devices and more complex circuitry to realize an active matrix organic light emitting display (AMOLED), which is generally recognized as the next generation FPD due to its wide color range, high contrast ratio, and thin/light display module [4].

In the last few years, tremendous progress has been made in amorphous metal oxide (AMO) TFTs, such as Zn-O [5], Zn-Sn-O [6], and In-Ga-Zn-O [7] TFTs. AMO TFTs posses certain advantages including visible transparency, good uniformity over large area, low processing temperature, decent mobility, sharp subthreshold swing, low off current, potentially better electrical stability, and are now viewed as a competitive technology for future FPDs. Several AMO TFT based AMOLEDs have also been demonstrated, indicating a promising future for these devices [8] [9]. In this paper, RF sputter a-InGaZnO TFTs were fabricated and characterized. Several methods of analyzing the TFT electrical properties were investigated, including the extraction of the field-effect mobility, threshold voltage, nonlinear factor, and source/drain contact resistance.

Experimental: Fig. 1 shows the top view and cross section of an inverted-staggered a-InGaZnO TFT used in this study [10]. The TFTs were fabricated on glass substrates. The gate electrode Ti (5nm)/Au (40nm)/Ti (5nm) was deposited by electron-beam and patterned by lift off. The gate insulator SiO_2 (200nm) and a-InGaZnO thin film were both deposited by RF sputtering and patterned by wet etch. After annealing in air at 300°C for 20 min, the source/drain electrodes Ti (5nm)/Au (40nm)/Ti (5nm) were deposited by electron-beam and patterned by lift off. A SiO_2 film as the back channel protection layer (100nm) was deposited by RF sputtering and patterned by wet etch. Finally, the TFTs were annealed in air at 200°C for 1 hour. Electrical measurements were done in dark using a Hewlett-Packard 4156A semiconductor parameter analyzer.

Results and TFT Parameter Extraction: The a-InGaZnO TFT output characteristics were measured by sweeping the drain-to-source voltage (V_{DS}) from 0 to 20V for various gate-to-source voltage (V_{GS}) levels as shown in Fig. 2 (a). The inset shows a closer view of the plot for lower V_{DS} voltages (0 ~ 1V). It can be observed that there is no current crowding near the origin of the output characteristics. Current crowding is a phenomenon which

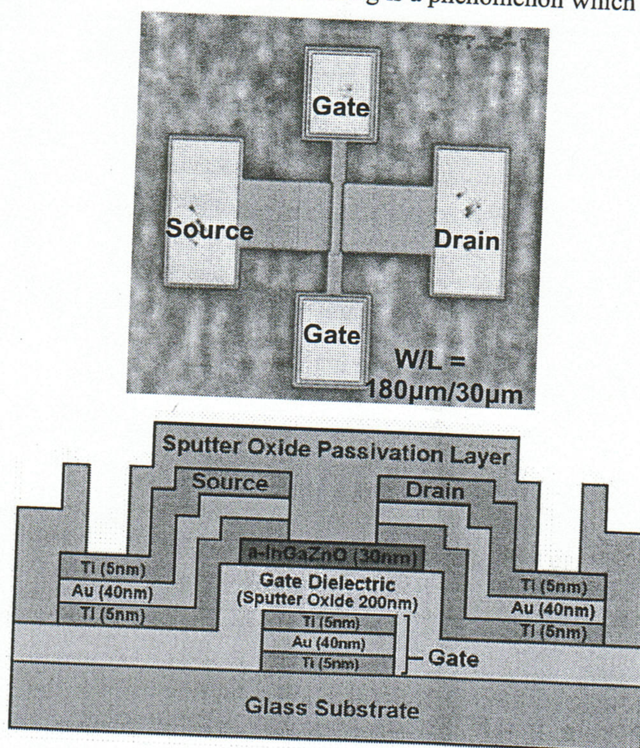

Figure 1. (a) Top view and (b) cross section of an RF sputter a-InGaZnO TFT used in this study.

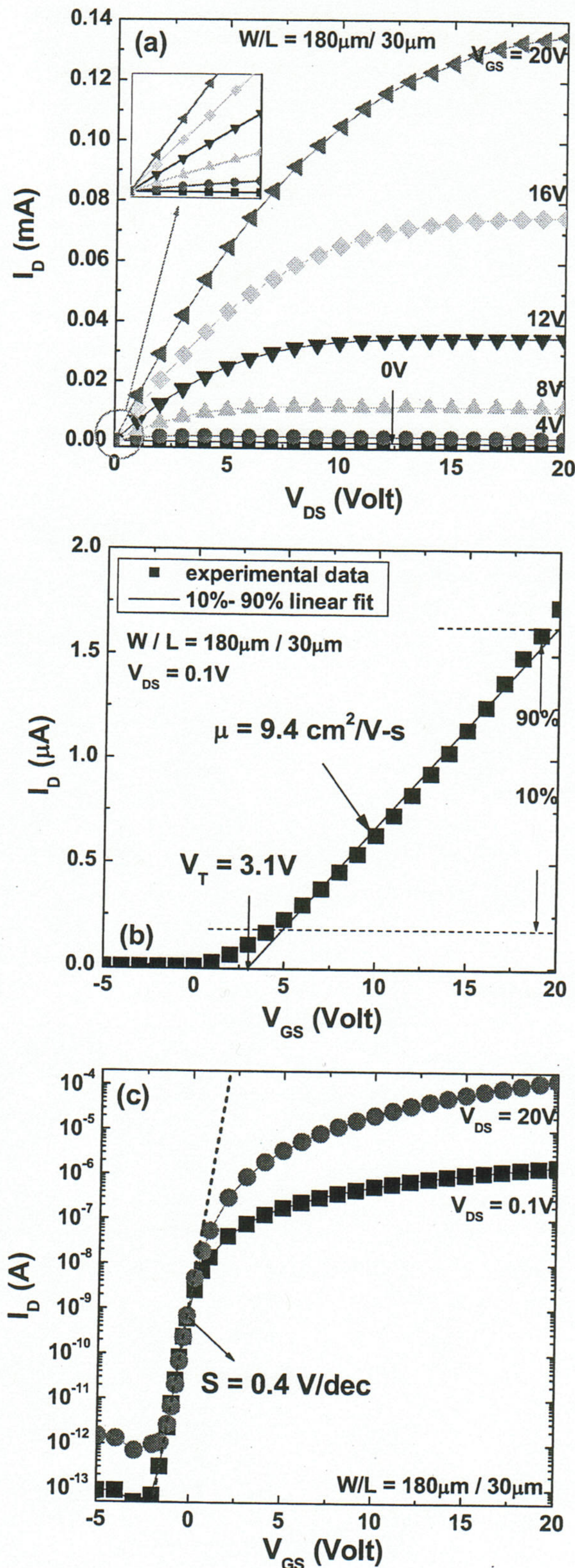

Figure 2. Measured (a) output characteristics, (b) linear regime transfer characteristics and (c) transfer characteristics plotted in log scale of RF sputter a-InGaZnO TFTs.

the drain current increases slowly with increasing V_{GS} such that the output characteristics for different V_{GS} appear to crowd together, and usually occurs when the source/drain contact is not Ohmic [11]. The output characteristics of our a-InGaZnO TFTs indicate that a sufficient on-current can be maintained even with very low V_{DS} voltages, which is desirable for AMFPD applications.

Fig. 2 (b) shows the measured TFT linear regime (V_{DS} = 0.1V) transfer characteristic. We extracted the apparent field-effect mobility (μ) and threshold voltage (V_T) by using the standard MOSFET equation.

$$I_D = \frac{W}{L} \cdot C_{ox} \cdot \mu \cdot (V_{GS} - V_T) \cdot V_{DS} \quad (1)$$

where W and L are the channel width and channel length, respectively, and C_{ox} is the gate insulator capacitance per unit area. To accommodate for the nonlinearity of our I_D-V_{GS} curve, a fitting range between 10% and 90% of the maximum measured I_D is chosen, as shown as the solid line in fig. 2 (b). We extracted from the x-interception and slope V_T = 3.1V and μ = 9.4 cm²/V-s, respectively.

Fig. 2 (c) shows the TFT transfer characteristics plotted in log scale for V_{DS} = 0.1V and 20V. Very low off-currents (10^{-13}~10^{-12}A), and current On-Off ratios exceeding 10^8 are achieved. The subthreshold slope (S) is extracted at the steepest point of the log(I_D)-V_{GS} plot by using the following equation

$$S = \left(\frac{d\log(I_D)}{dV_{GS}} \right)^{-1} \quad (2)$$

The subthreshold slope of our a-InGaZnO TFTs is extracted to be as small as ~0.4V/dec, which allows achieving a high switching speed with a low gate driving voltage. The above mentioned electrical properties (decent mobility, sharp subthreshold slope, low off-currents) make a-InGaZnO TFTs very favorable for future AMFPD applications.

V_{GS} Dependent Field-Effect Mobility: The standard MOSFET equation assumes a linear relation between I_D and V_{GS}, which is not valid for our a-InGaZnO TFTs, as can be seen from fig. 2(b). This nonlinearity can be better observed by extracting the apparent field-effect mobility (μ) from the first derivative of the linear regime I_D-V_{GS} curve

$$\mu = \frac{\partial I_D / \partial V_{GS}}{W/L \cdot C_{ox} \cdot V_{DS}} \quad (3)$$

The apparent field-effect mobility (μ) as a function of V_{GS} is plotted in Fig. 3(b). We can see that instead of maintaining a constant value, μ increases with V_{GS} and reaches a maximum value of 12.2cm²/V-s within our measurement range, and the apparent field-effect mobility extracted by (1) can in fact be considered as an average of that extracted by (3). We believe that this V_{GS} dependence of μ can be explained by the energy dependent, density-of-localized-states near the Fermi level. As V_{GS} increases,

most localized states are filled, and more induced charges can contribute to the free carriers (I_D) [12].

To better model the a-InGaZnO TFT I-V characteristics, a V_{GS} dependent field-effect mobility can be introduced

$$\mu = \mu_0 \cdot (V_{GS} - V_T)^{\gamma} \qquad (4)$$

where μ_0 is the fitting parameter associated with the field-effect mobility and γ is the nonlinearity factor. It should be noticed that the unit of μ_0 is $cm^2/V^{1+\gamma}$-s, therefore the unit of μ can be maintained at cm^2/V-s.

By plugging (4) into (1), the MOSFET equation becomes

$$I_D = \frac{W}{L} \cdot C_{ox} \cdot \mu_0 \cdot (V_{GS} - V_T)^{1+\gamma} \cdot V_{DS} \qquad (5)$$

The parameters V_T, μ_0, and γ can be extracted by fitting equation (5) to the TFT linear regime transfer characteristic, as shown as the solid line in Fig. 3 (a). The obtained values are V_T = 0.22V, μ_0 = 2.36 $cm^2/V^{1+\gamma}$-s, and γ = 0.43. The field-effect mobility extracted by (4) is plotted in Fig. 3(b).

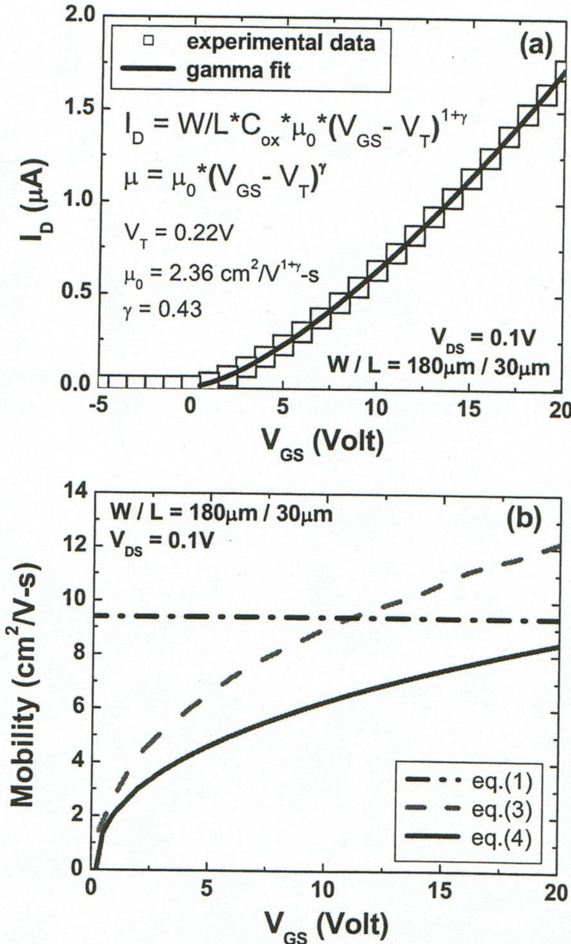

Figure 3. (a) Extracting the field-effect mobility and threshold voltage by considering the non-linearity of the TFT I-V curve (b) The V_{GS} dependence of the field-effect mobility (μ) extracted by eq.(1), (3) and (4).

Although the μ extracted by (3) and (4) are both V_{GS} dependent, (3) does not take into consideration the nonlinearity of the I_D-V_{GS} curve, and therefore overestimates the field-effect mobility by a factor of 1+ γ compared to the gamma method.

$$\frac{\partial I_D / \partial V_{GS}}{W/L \cdot C_{ox} \cdot V_{DS}} = (1+\gamma) \cdot \mu_0 \cdot (V_{GS} - V_T)^{\gamma} \qquad (6)$$

Source/drain Contact Resistance: We investigated the source/drain contact resistance (R_S/R_D) of the a-InGaZnO TFTs by using the transmission line method (TLM) [13]. The total TFT ON resistance (R_T) can be described by

$$R_T = \frac{V_{DS}}{I_D} = R_S + R_D + r_{ch} \cdot L \qquad (7)$$

where r_{ch} is the TFT channel resistance per unit length. Using equations (1) and (7), we can express the total TFT ON resistance R_T as a function of the apparent field-effect mobility (μ) and threshold voltage (V_T).

$$R_T = \frac{V_{DS}}{I_D} = \frac{L}{W \cdot C_{ox} \cdot \mu \cdot (V_{GS} - V_T)} \qquad (8)$$

Applying the same equation to the ideal TFT (conduction channel only, without R_S/R_D) allows us to express the TFT channel resistance per unit length r_{ch} as a function of the intrinsic mobility (μ_{in}) and threshold voltage (V_{Tin})

$$r_{ch} = \frac{1}{W \cdot C_{ox} \cdot \mu_{in} \cdot (V_{GS} - V_{Tin})} \qquad (9)$$

The intrinsic TFT parameters μ_{in} and V_{Tin} are representative of the electrical characteristics of the conduction channel without the influence of the source/drain contact resistance.

We applied the TLM to our a-InGaZnO TFTs by analyzing a series of TFTs with the same channel width (180μm) but different channel lengths (10μm, 30μm, 60μm). The apparent TFT parameters are summarized in Table 1. The apparent threshold voltage (V_T), subthreshold slope (S), and off-current values (I_{OFF}) are similar for the 3 TFTs, while the apparent field-effect mobility (μ) slightly increases with the channel length. This channel length dependence of μ is due to the effect of R_S/R_D, which will be clearer later on. The extraction of the TFT source/drain contact resistance and intrinsic field-effect mobility and threshold voltage is then rather straightforward. We first plot R_T as a function of the TFT channel length for different V_{GS}, as shown in Fig. 4. By fitting the R_T-L plot to equation (7), $R_S + R_D$ and r_{ch} can thus be obtained from the y-interception and slope for different V_{GS} biases, respectively. The extracted source /drain contact resistance ($R_S + R_D$) and channel resistance ($r_{ch} \times L$) are both V_{GS} dependent as shown in Fig. 5. $R_S + R_D$ is 1.7kΩ at V_{GS} = 20V and increases to 23 kΩ at V_{GS} = 4V, and is more than one order of magnitude smaller than the TFT channel resistance, depending on the channel

length. The intrinsic TFT parameters can then be obtained by plotting $1/r_{ch}$ versus V_{GS}, as shown in Fig. 6. Using equation (9), V_{Tin} and μ_{in} can be extracted by the x-interception and the slope, respectively. The data shown in Fig. 6 yield $V_{Tin} = 3.5V$ and $\mu_{in} = 8.8cm^2/V\text{-}s$. It can be observed from Table 1 that the TFT apparent field-effect mobility is slightly smaller than its intrinsic value. This effect is more severe for shorter channel length devices, since the channel resistance is smaller and therefore more comparable to the source/drain contact resistance.

Table. 1 The field-effect mobility (μ), threshold voltage (V_T) , subthreshold slope (S), and off-current (I_{OFF}) of TFTs with different channel length.

L (μm)	10	30	60
μ (cm^2/V-s)	7.7	7.94	8.16
V_T (V)	3.2		
S (V/dec)	0.4		
I_{OFF} (A)	$10^{-13} \sim 10^{-12}$		

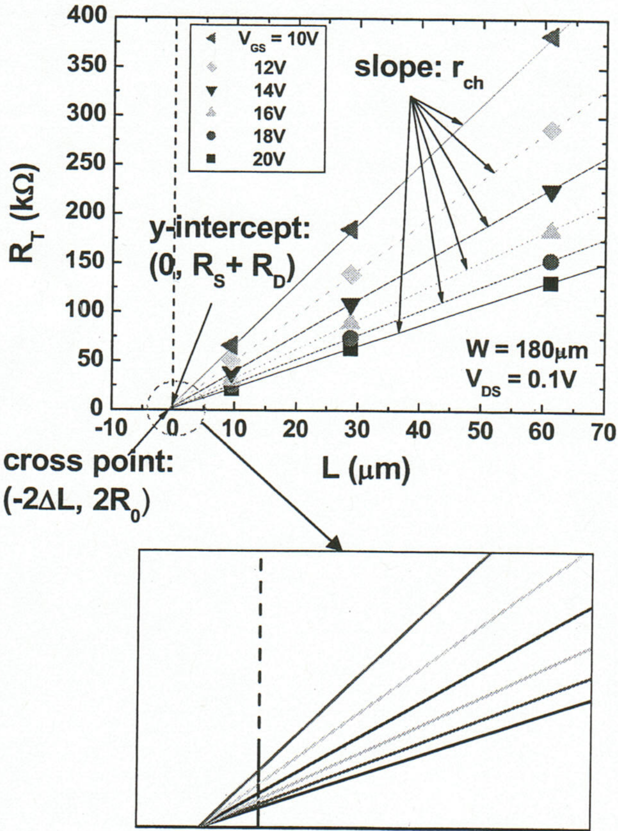

Figure 4. The total TFT ON resistance (R_T) versus channel length (L) for several levels of V_{GS}. The TFT channel resistance per unit length (r_{ch}) and contact resistance (R_S+R_D) are extracted from the slope and y-intercept of the plots for different V_{GS}, respectively. ΔL and R_0 are extracted from the common cross point of all R_T – L curves.

The effect of the source/drain contact resistance can also be represented as an increase of the apparent channel,

$$R_T = R_S + R_D + \frac{L}{W \cdot C_{ox} \cdot \mu_{in} \cdot (V_{GS} - V_{Tin})} = 2 \cdot R_0 + \frac{L + 2 \cdot \Delta L}{W \cdot C_{ox} \cdot \mu_{in} \cdot (V_{GS} - V_{Tin})} \quad (10)$$

where R_0 represents the limit of R_S/R_D for a very high V_{GS}, and ΔL is associated with the effective channel length. Both ΔL and R_0 are independent of V_{GS}. The values of ΔL and R_0 are extracted from the common cross point of the R_T-L curves, whose coordinate is (-2 ΔL, 2 R_0), as shown in Fig. 4. We obtained ΔL ~ 0.5μm, which indicates that the effective channel length is longer than the physical channel length (the current path extends beyond the source/drain contact edges), and R_0 ~ 0Ω, which implies a negligible source/drain contact resistance at very high V_{GS} voltages.

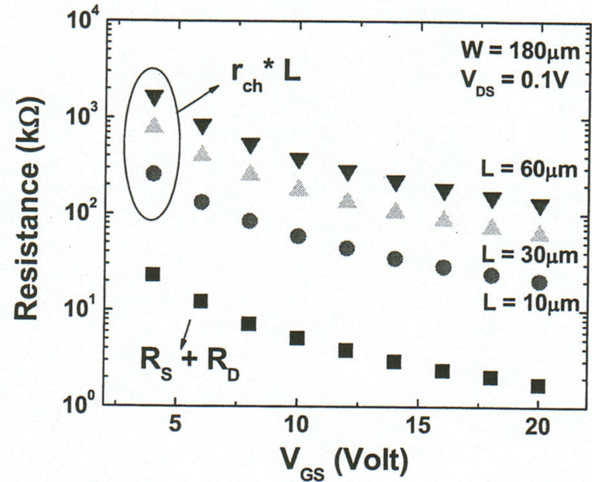

Figure 5. The Contact resistance ($R_S + R_D$) and the channel resistance (r_{ch}* L) as a function of V_{GS}.

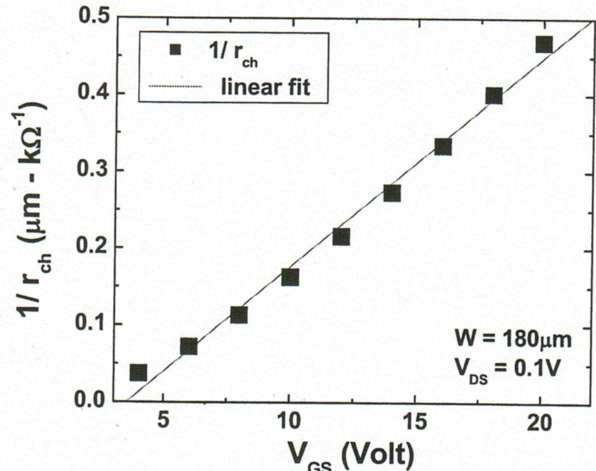

Figure 6. Extracting the intrinsic field-effect mobility and threshold voltage by plotting $1/r_{ch}$ versus V_{GS}.

It should be noticed that although the standard MOSFET equation is used in eq. (8) ~ eq. (10), the nonlinear factor (γ) can also be included to take into consideration the nonlinearity of I_D-V_{GS}.

Conclusion: We fabricated inverted-staggered RF-sputter a-InGaZnO TFTs on glass substrate. We characterized their basic electrical properties, and several extraction methods were suggested. We also investigated the source/drain contact resistance of the TFTs. The a-InGaZnO TFTs overall demonstrated high field-effect mobilities, low off-currents, and sharp subthreshold slopes, which make them very suitable for future display backplane devices.

References

1. M. Kimura, I. Yudasaka, S. Kanbe, H. Kobayashi, H. Kiguchi, S. Seki, S. Miyashita, T. Shimoda, T. Ozawa, K. Kitawada, T. Nakazawa, W. Miyazawa, H. Ohshima, "Low-temperature polysilicon thin-film transistor driving with integrated driver for high-resolution light emitting polymer display," *IEEE Trans. on Electron Devices*, vol. 46, no. 12, pp. 2282-2288, 1999.
2. M.K. Hatalis, M.J. Stewart, and R.S. Howell. "Advanced polysilicon TFT technology for active matrix organic light-emitting diode displays," *Proceedings of the SPIE - The International Society for Optical Engineering,* vil 3363, pp. 278-287, 1998.
3. D. Striakhilev, A. Nathan, Y. Vygranenko, P. Servati, C.H. Lee, A. Sazonov, "Amorphous silicon display backplanes on plastic substrates," *Journal of Display Technology*, vol. 2, no. 4, pp. 364-371, 2006.
4. C. W. Tang, "An overview of organic electroluminescent materials and devices," *J. of SID*, vol. 5, no. 1, pp. 11-14, 1997.
5. R.L. Hoffman, B.J. Norris, J.F. Wager, "ZnO-based transparent thin-film transistors," *Applied Physics Letters,* vol. 82, no. 5, pp. 733-735, 2003.
6. H.Q. Chiang, J.F. Wager, R.L. Hoffman, J. Jeong, D.A. Keszler, "High mobility transparent thin-film transistors with amorphous zinc tin oxide channel layer," *Applied Physics Letter,* vol. 86, no. 1, 13503, 2005.
7. K. Nomura, H. Ohta, A. Takagi, T. Kamiya, M. Hirano and H. Hosono, "Room-temperature fabrication of transparent flexible thin-film transistors using amorphous oxide semiconductors," *Nature,* vol. 432, pp. 488-492, 2004.
8. J. Y. Kwon, K. S. Son, J. S. Jung, T. S. Kim, M. K. Ryu, K. B. Park, J. W. Kim, Y. G. Lee, C. J. Kim, S. I. Kim, Y. S. Park, S. Y. Lee and J. M. Kim, "4 inch QVGA AMOLED display driven by GaInZnO TFT," *Int. Display Workshop*, AMD9-3, 2007, p. 1783.
9. J. K. Jeong, J. H. Jeong, J. H. Choi, J. S. Im, S. H. Kim, H. W. Yang, K. N. Kang, K. S. Kim, T. K. Ahn, H. J. Chung, M. Kim, B. S. Gu. J. S. Park, Y. G. Mo, H. D. Kim, and H. K. Chung, '12.1-Inch WXGA AMOLED Display Driven by Indium-Gallium-Zinc Oxide TFTs Array," *SID 2008*, 3.1.
10. K. Abe, H. Kumomi, K. Nomura, T. Kamiya, M. Hirano, and H. Hosono, "Amorphous In-Ga-Zn-O based TFTs and circuits," *Int. Display Workshop*, AMD9-2, pp. 1779-1782, 2007.
11. J. Kanicki, F. R. Libsch, J. Griffith, and R. Polastre, "Performance of thin hydrogenated amorphous silicon thin-film transistors," *J. Appl. Phys.*, vol. 69, pp. 2339-2345, 1991.
12. S. Kishida, Y. Naruke, Y. Uchida and M. Matsumura, "Theoretical Analysis of Amorphous-Silicon Field-Effect-Transistors," *Jpn. J. Appl. Phys.* vol. 22, pp. 511-517, 1983.